# Nanojoule-Energy-Level, Polarization-Maintaining, Dissipative-Soliton Mode-Locked Thulium Fiber Laser at 1876 nm

Panuwat Srisamran <sup>a</sup>, Ibrahim Abughazaleh <sup>a</sup>, Matthew Gerard <sup>a</sup>, Duanyang Xu <sup>a</sup>, Yongmin Jung <sup>a</sup>, Jing He <sup>b</sup>, Jeremiah Marcellino <sup>b</sup>, Boyang Mao <sup>b</sup>, Andrea C. Ferrari <sup>b</sup>, David Richardson <sup>a</sup>, and Lin Xu <sup>a,\*</sup>

**Abstract:** We report an environmentally robust, dissipative-soliton, mode-locked Tm-doped fiber laser operating in the short-wavelength infrared region at 1876 nm, using all-polarization-maintaining (all-PM) fibers. Self-starting, mode-locked operation is enabled by a single-wall carbon nanotube (SWNT) based saturable absorber (SA). Cavity dispersion is managed by using a commercially available PM dispersion compensating fiber (DCF). A PM fiber Lyot filter enables dissipative-soliton mode locking at a central wavelength of 1876 nm. The laser generates stable pulses at a repetition rate~19.2 MHz with an average power~21.5 mW, corresponding to a pulse energy~1.1 nJ. The output pulse has a duration of 4.2 ps and can be compressed down to 391 fs using a grating-based compressor. A higher pulse energy~3.2 nJ can be obtained with a compressed pulse width of 566 fs by varying the net cavity dispersion. To the best of our knowledge, this is the first nJ-energy-level, all-fiberized PM dissipative-soliton mode-locked Tm-doped fiber laser based on SWNT, with potential for applications in high-penetration nonlinear biomedical imaging microscopy.

Keywords: Mode-locked Tm fiber laser; Polarization maintaining fiber; Dissipative soliton; Short-wavelength infrared

#### 1. Introduction

Ultrafast Tm-doped fiber lasers (TDFLs) operating in the 2-µm region have gained great interest due to their ability to support several applications including spectroscopy [1], material processing [2], and remote sensing [3]. In medical microscopy applications, (tens-hundreds) femtosecond (fs) pulses in the short-wavelength infrared (SWIR) region (~1650-1900 nm) have a great potential to be used for deep (mm) penetration imaging in general biological tissues [4], due to their nature of high optical transparency comparing to other wavelength regions [5]. They can be used for multiphoton microscopy imaging in biomedical research [4, 5]. Tm-doped fibers provide broad emission wavelengths from ~1650 to 2100 nm [6] that cover the SWIR region. Mode-locking TDFLs to produce ultrashort pulses at wavelengths <1900 nm requires a balanced management of signal gain and reabsorption due to the quasi-three-level nature of the Tm-doped fiber [7]. Moreover, there is limited availability of accessible saturable absorber (SA) materials designed for the wavelengths within the SWIR region [8]. Hence, development of femtosecond-pulsed, nanojoule-energy, mode-locked (ML) TDFLs operating in the SWIR can be challenging.

ML-TDFL generating ultrashort (150 fs) pulses at 1820 nm was reported for 3-photon fluorescence microscopy [9]. However, free-space components were used in the laser system due to splice difficulty between the fluoride-glass fiber and standard silica-glass fibers, which would pose challenges to deployment for practical applications. An all-fiberized ML-TDFL operating at 1840 nm was developed with silica-glass fibers and demonstrated for third-harmonic generation microscopy in biomedical samples [10]. However, non-polarization-maintaining (non-PM) fibers were use in the ML-TDFL, and these non-PM fibers are typically sensitive to environmental temperature variations and physical perturbations in maintaining polarization state, leading to the variation of output pulse properties i.e. spectral bandwidth, pulse duration or energy [11]. Non-PM cavities generally require adjustment of a polarization controller to resume and maintain mode-locked operation if they experience external perturbation [12]. In contrast, ML lasers based on PM fibers offer robustness and stability [13], thanks to the high (in the order of 10<sup>-4</sup>) birefringence of PM fibers [14], which is insensitive to environment conditions [15], maintaining a single polarization without the requirement of any controlling mechanism [16]. Therefore, ML lasers with PM-fiber cavities are the preferred solution for reliable sources.

Several all-PM ML-TDFLs were reported using different SAs, including optical loop mirrors [17], graphene [18], carbon nanotubes (CNTs) [19], and semiconductor saturable absorber mirror (SESAM) [20]. They were

<sup>&</sup>lt;sup>a</sup> Optoelectronics Research Centre, University of Southampton, Southampton, SO17 1BJ, United Kingdom

<sup>&</sup>lt;sup>b</sup> Cambridge Graphene Centre, University of Cambridge, Cambridge, CB3 0FA, United Kingdom

<sup>\*</sup>Corresponding author email: l.xu@soton.ac.uk

based on all-anomalous dispersion cavities and produced conventional solitons with low pulse energies in the pJlevel due to the anomalous dispersion of standard single mode fiber (SMF) in the 2-µm region [21]. Dispersion managed cavities, in which dispersion compensating fibers (DCFs) with normal dispersion alter the intra-cavity dispersion, can reduce nonlinear phase accumulation to provide higher pulse energies [12]. However, managing dispersion in all-PM ML-TDFLs is challenging due to the limited availability of PM-DCFs [22, 23]. Ref. [22] reported a dispersion-managed PM ML-TDFL cavity using an 1.5-m-length, in-house-fabricated, PM-DCF and a 35-layer graphene/poly(methyl methacrylate)-based SA. However, the ML-TDFL operated at 1945 nm, generating a maximum output pulse energy of only 220 pJ. Ref. [23] demonstrated a PM ML-TDFL cavity using a 0.7m, commercial PM-DCF (PM2000D, Coherent) and an arc-discharge, single-wall nanotube (SWNT)-based SA. Although the ML-TDFL operated at 1787 nm, the output pulse energy was quite low (~70 pJ). Despite PM-DCFs being employed in these cavities, the net-cavity dispersions remained in the anomalous-dispersion region [22, 23], resulting in stretched-pulse mode locking with pJ-level output pulse energies. Dissipative-soliton ML cavities with net-cavity dispersions in the normal-dispersion region offer greater tolerance to nonlinear phase shifts than other soliton types [24]. Hence, they are capable of producing output pulse energies at the nJ-level [25]. However, net-normal dispersion ML operation depends not only on a balanced conservative effect between dispersion and nonlinearity [26], but also on the dissipative effects between spectral gain and loss [25]. Therefore, dissipative-soliton cavities require careful control of dispersion and proper selection of the spectral filter. Ref. [27] reported a dissipative-soliton ML-TDFL constructed with all-PM fibers. A 3m-long specially designed and inhouse-fabricated PM-TDF was employed acting as both gain fiber and DCF. Dissipative-soliton mode locking was realized. However, the operating wavelength was 1995nm, and the output pulse energy was very low (~44 pJ), due to high (~3 dB) splicing losses between PM-TDF and standard PM-SMFs in the cavity.

Here, we present an all-fiberized dissipative-soliton PM ML-TDFL operating in the SWIR delivering nJ-level output pulse energies. SWNT samples are fabricated and used as a SA, while a bandpass filter constructed with PM fibers enables the dissipative-soliton ML operation. The laser has excellent performance, including being self-starting, and environmentally insensitive, and generating dissipative solitons at 1876 nm with pulse energies >1 nJ. The output pulses have a duration of 4.2 ps and can be compressed down to 391 fs with an external grating-based compressor. To the best of our knowledge, this is the first nJ-level all-PM dissipative-soliton ML-TDFL operating below 1900 nm utilizing a commercially available DCF and a SWNT-SA. This turn-key ML laser exhibits stable mode-locking performance and output power, making it a reliable source for multiphoton microscopy in biomedical applications.

# 2. Experiments

# 2.1 Mode-Locked Cavity Design

A schematic of the all-PM ML-TDFL cavity is in Fig. 1. A continuous-wave (CW) laser seeded Er-doped fiber amplifier (EDFA; EAD-5K-C, IPG Fibertech) is used as a pump source at 1563 nm, with a maximum output power of 7 W. The CW pump light is coupled into the cavity through a 1560/1876 nm PM wavelength division multiplexer (WDM). A short (8 cm) length of PM Tm-doped fiber (TDF; PM-TSF-5/125, Coherent) enables operation in the SWIR. The unabsorbed pump light is filtered by another WDM placed following the TDF. A PM output coupler (OC) with a 90% output coupling ratio is used to extract the mode-locked pulses at maximum efficiency. A fast-axisblocked PM-isolator (PMI) acts as a linear polarizer and ensures unidirectional ring oscillation. A Lyot filter (LF) [28], constructed from PM fibers, provides the intracavity spectral filtering necessary to facilitate dissipative-soliton mode locking. A 11-cm PM-SMF is spliced between the OC and PMI tails with a 45° rotation relative to the principal axis of the fiber to excite two different polarization components and introduce a phase delay. This relative phase delay is wavelength-dependent, enabling the creation of a spectral filter by controlling the PM-SMF length. Another identical section of PM-SMF, with a length equal to the input fiber tail of the PMI, is spliced with a 90° rotation offset to the PMI. This compensates for polarization-dependent GVD in the PMI fiber, preventing pulse walk-off effects [29, 30]. Fig. 2(a) shows the fiberized LF structure. The red line of Fig. 2(b) plots the transmission spectrum of the LF with a wideband ASE source, revealing a periodic bandpass function with a peak wavelength around 1876 nm, a free-spectral range of 72 nm and a full-width at half-maximum (FWHM) bandwidth of 36 nm, consistent with the calculated FWHM bandwidth of 37.7 nm [31, 32]. The LF insertion loss was measured to be ~0.4 dB around the peak wavelength. The wavelength-dependent transmission of the LF can be adjusted by changing the birefringence of the LF fiber using temperature control or tension variation [33, 34]. A SWNT-polyvinyl alcohol (PVA) composite [35] is placed between two angled fiber patch cords at the PMI output, serving as a SA.

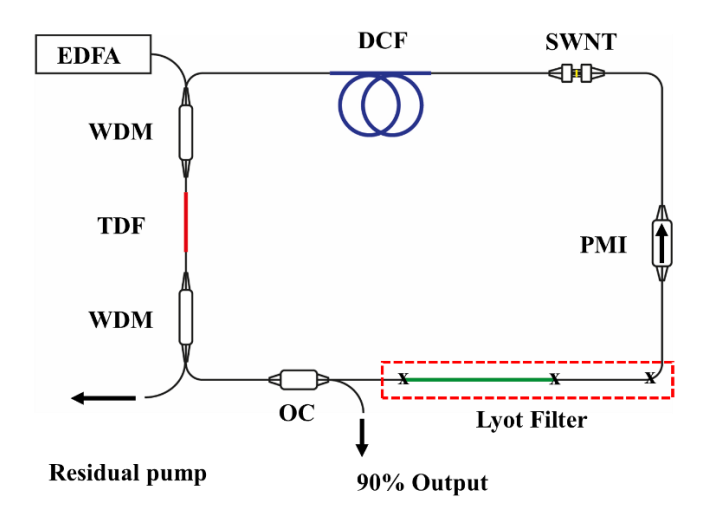


Fig. 1. Schematic of all-PM Tm-doped fiber dissipative soliton laser.

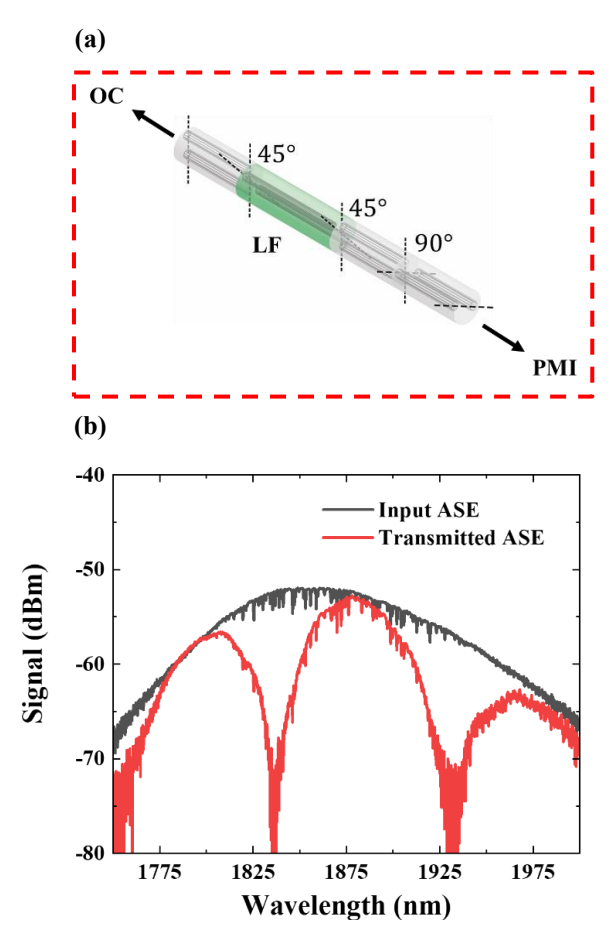


Fig. 2. (a) Schematic of Lyot filter (LF) and (b) input and transmitted ASE spectrum of our Lyot filter.

A 4m long PM-DCF (PM2000D, Coherent) is used to manage the intra-cavity dispersion. The DCF has a measured birefringence of  $1.54 \times 10^{-4}$ , approximately half that of the PM-SMF. There is a significant core size mismatch (2.1-µm vs 8.5-µm) between DCF and SMF, requiring special care during splicing and handling to minimize splicing losses, and enhance the PM performance of the DCF. To mitigate these issues, short (<10 cm) sections of PM1950 (Coherent) fiber are used as bridge fibers to reduce splicing losses and improve the PM performance within the cavity. Compared with direct splicing of PM-DCF with PM-SMF, splicing losses are reduced by 2.5 dB using the bridge fibers. The total insertion losses of the PM-DCF in the cavity is 1.7 dB. The cavity has a total fiber length of 10.6 m with an estimated net dispersion of 0.01 ps² (TDF:  $\beta_2$  = -0.02 ps²/m; SMF:  $\beta_2$  = -0.059 ps²/m; PM1950:  $\beta_2$  = -0.02 ps²/m DCF:  $\beta_2$  = 0.098 ps²/m) [36, 37].

## 2.2 Carbon Nanotube Saturable Absorber Characterization

The SA is designed for operation in the SWIR. SWNT-PVA composites are prepared [35] using semiconducting SWNTs with a mean diameter of 1.4 nm (Nanointegris). From Raman spectroscopy, we determine the radial breathing mode (RBM) positions, related to the SWNT diameter, dt [38] as  $Pos(RBM) = C_1 / dt + C_2$ . Here, we use  $C_1 = 214.4 \text{ cm}^{-1}$  and  $C_2 = 18.7 \text{ cm}^{-1}$  from Ref [38], derived from plotting the resonance energy as a function of inverse Pos(RBM) without additional assumptions. The RBM spectra of the powders [Fig. 3(b)] (black line) show a broad distribution, spanning 150–174 cm<sup>-1</sup>, corresponding to SWNTs with diameters~1.3-1.6 nm. Fig. 3(c, d) display a weak D band [I(D)/I(G) = 0.04], indicating a defects [39].

The absorption spectrum of the SWNT-PVA composite is in Fig. 3(a) (blue line), revealing an absorption band between 1.6 and 2.1  $\mu$ m, corresponding to  $eh_{11}$  excitonic transitions of SWNTs with diameters in the 1.2–1.7 nm range [40]. The PVA absorption is negligible, being over an order of magnitude lower than the SWNT-PVA composite, in the 800 - 2400 nm range.

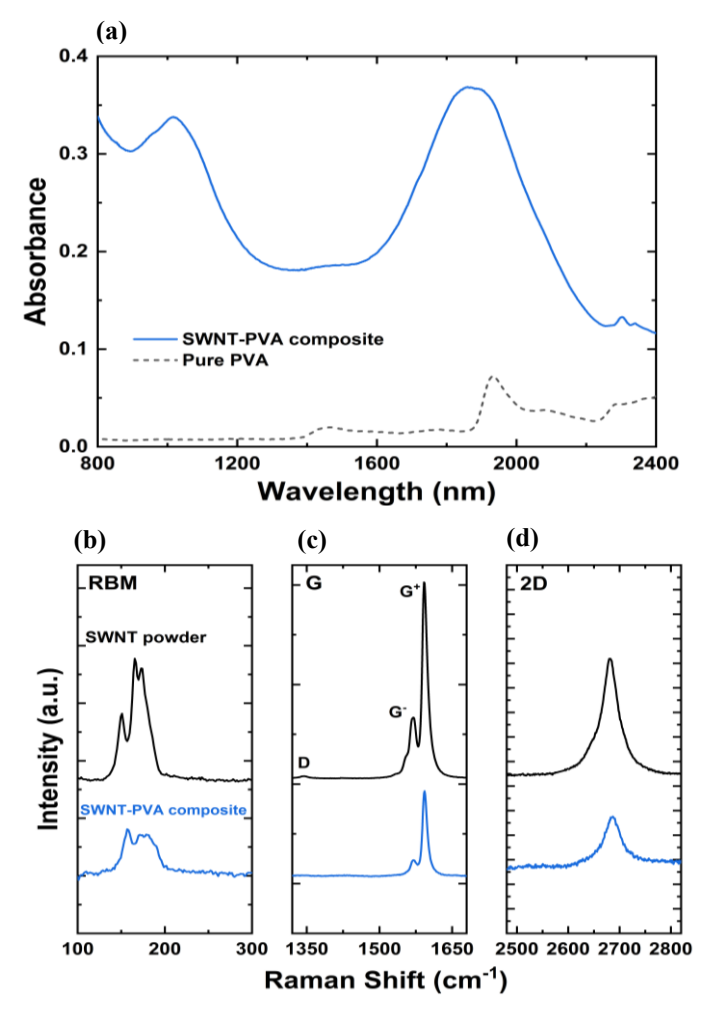


Fig. 3. (a) Absorption of SWNT-PVA composite (blue line), and pure PVA (black dash). (b,c,d) Raman spectra of SWNT powder (black lines) and SWNT-PVA composite (blue lines) at 514 nm excitation. (b) RBM region, (c) G region, (d) 2D region.

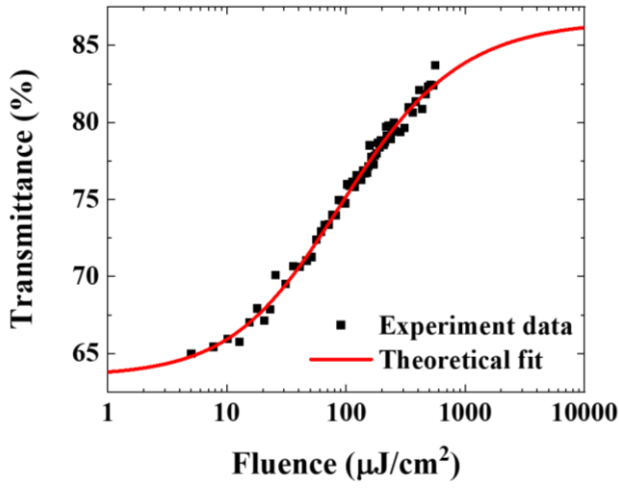


Fig. 4. Nonlinear transmission of SWNT-PVA composite.

The SA nonlinear transmission is characterized using a home-built ML-TDFL with a central wavelength of 1870 nm and a pulse duration of 600 fs as the pump source. Fig. 4 displays the measured nonlinear transmission of the SA (black dot) alongside its fitting using a fast saturable absorption model (red line) [19, 41]. The SA exhibits a modulation depth of 23.1% and a saturation fluence of  $56.1 \, \mu J/cm^2$ .

# 3. Results and Discussions

## 3.1 Dissipative Soliton Output Pulse Properties

ML self-starts at a threshold pump power of 870 mW, yielding an output power of 7.2 mW. Stable single-pulse ML is maintained up to 950 mW pump power. The output power increases linearly with pump power, exhibiting a slope efficiency of 17.9% and reaching a maximum power of 21.5 mW, Fig. 5. ML becomes unstable at higher pump powers. The output spectra at different powers are measured using an optical spectrum analyzer (AQ6375, Yokogawa). Fig. 6 shows the output spectra at various pump powers, displaying a sharp-edge spectral shape typical of dissipative-solitons [12, 42]. The spectral bandwidth gradually increases with output power, showing a central wavelength of 1876 nm with a 3-dB bandwidth of 26 nm at maximum output power.

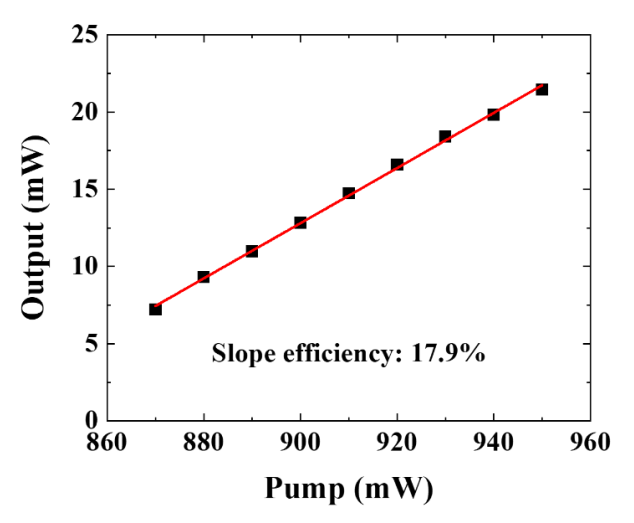


Fig. 5. Output power at different pump powers.

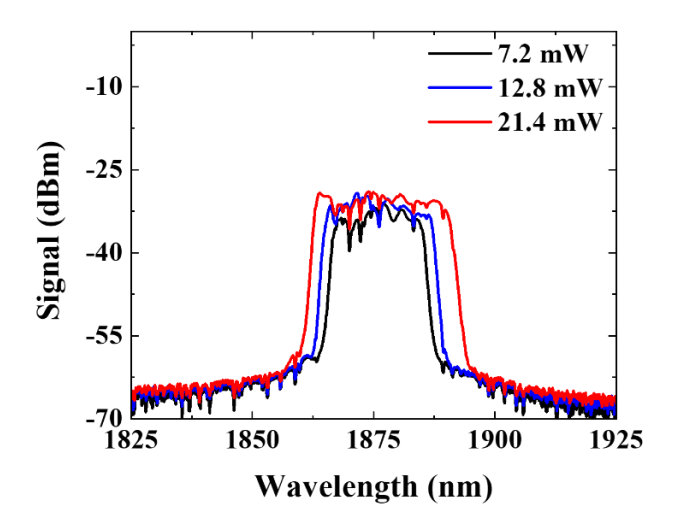


Fig. 6. Output spectra at different laser powers.

Radio frequency (RF) spectra are recorded with an InGaAs photodiode (ET-5000F, EOT) and a RF spectrum analyzer (RSA3303A, Tektronix) to characterize the ML stability. Fig. 7(a) presents a typical RF spectrum measured with a 200 Hz resolution, showing a fundamental frequency of 19.2 MHz with a signal-to-noise ratio (SNR)~71 dB. The repetition rate corresponds to the cavity length and the high SNR indicates stable single-pulse ML operation. The RF spectrum across a 1-GHz bandwidth is shown in Fig. 7(b), indicating no parasitic instabilities. The intensity drop in RF spectrum at higher-order harmonic, compared to the fundamental frequency, is primarily due to the limited detection bandwidth in the RF spectrum measurement, particularly the slow time response of the aged photodiode available for use. The maximum pulse energy is calculated to be 1.1 nJ.

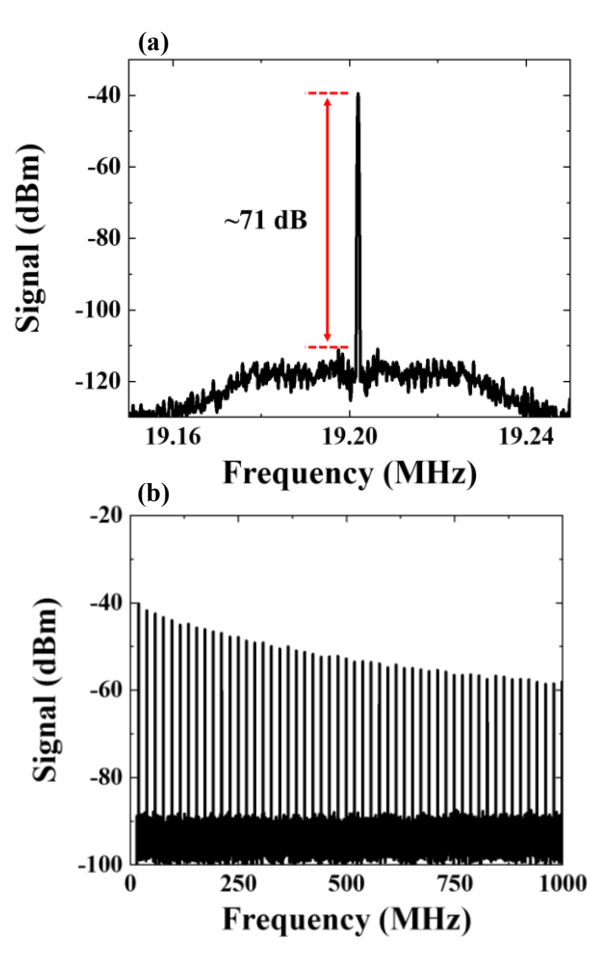


Fig. 7. RF spectrum of the output signal with (a) 100 kHz span at the fundamental frequency and (b) with 1 GHz span.

The output pulse duration is characterized using a non-colinear second-harmonic generation autocorrelator

(pulseCheck NX150, APE). Fig. 8(a) presents a measured autocorrelation trace (black line) that matches well with a Gaussian pulse-shape fitting (red line), showing a FWHM~5.9 ps. Hence, the deconvolution pulse duration is around 4.2 ps. A pulse compressor consisting of a pair of transmission gratings with a grating density of 900 line/mm de-chirps the pulses. Fig. 8(b) shows a shortest pulse duration of 391 fs. The compressed pulse duration is 1.96 times larger than the calculated transform-limited pulse. This could be caused by nonlinear chirp not compensated by gratings [43], which could be improved by managing higher-order dispersions in the cavity [44].

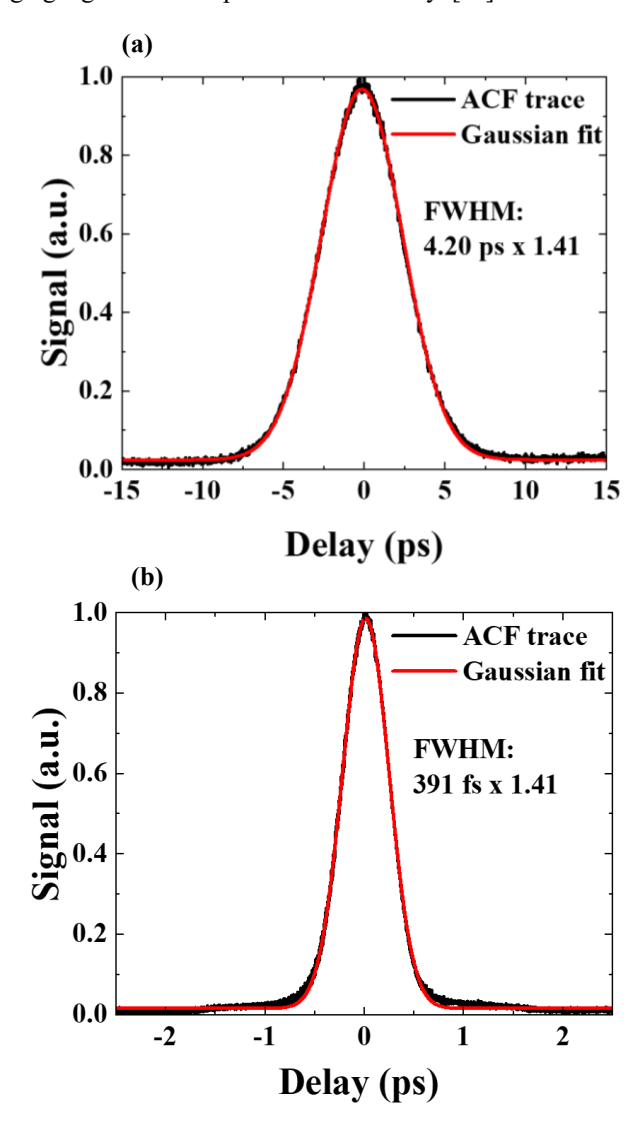


Fig. 8. Autocorrelation of (a) uncompressed pulses and (b) pulses after compressor.

# 3.2 Net Cavity Dispersion Variation

The net-cavity dispersion is adjusted by changing the length of the SMF to 0.03 and 0.06 ps², with a total cavity length of 10.2 and 9.7 m, respectively. Accordingly, the fundamental repetition rate shifts to 20 and 21.1 MHz. Fig. 9(a) shows the minimum compressed pulse durations and the maximum pulse energies for the different dispersion conditions. With a larger positive dispersion, the cavity can tolerate a higher pump power before the onset of multipulsing, and generates a higher output power [12]. E.g., for 0.06 ps², the maximum pump power increases to 1.2 W, with a maximum output pulse energy of 3.2 nJ for single-pulse ML operation. However, the output pulses have a narrower spectrum (20 nm), leading to a longer compressed pulse width (566 fs). Autocorrelation traces with Gaussian fitting for pulses at energies of 2.4 nJ and 3.2 nJ are presented in Fig. 9(b) and (c), respectively. It was possible to achieve a higher pulse energy with a further increase in the net-cavity dispersion, however, re-optimization of Lyot filter bandwidth would be needed to balance the higher dispersion for the dissipative soliton operation. Furthermore, constrains from power handling of the fiber components and the saturable absorber would limit the power scaling of the mode-locked laser.

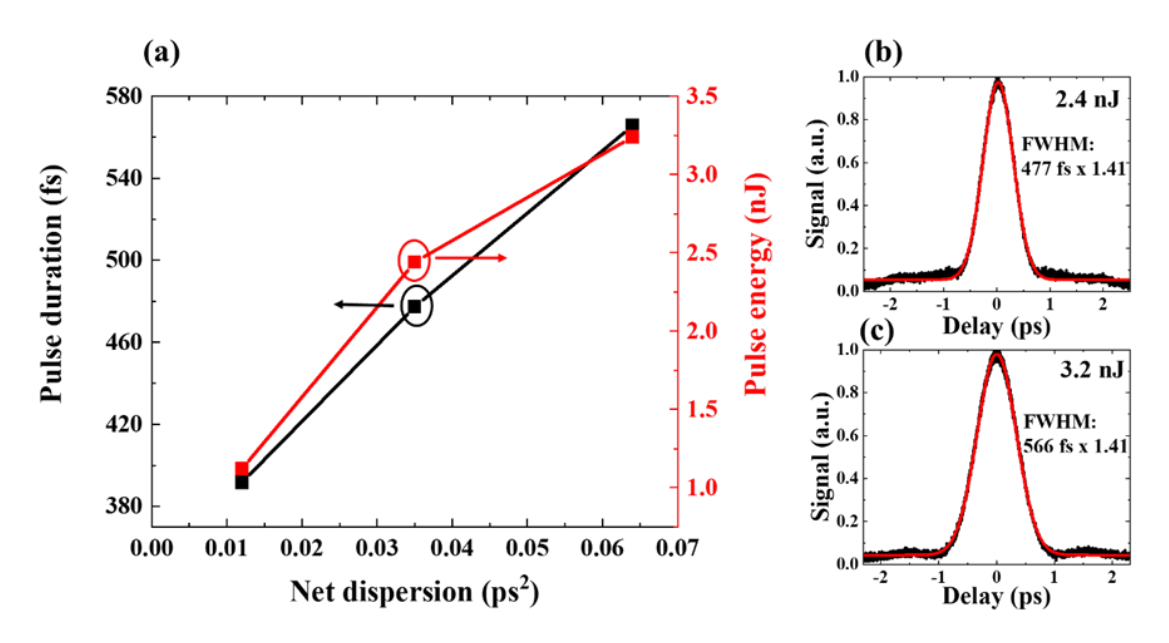


Fig. 9. (a) Compressed pulse durations and maximum pulse energies with various net cavity dispersions, autocorrelation trace along with Gaussian fitting for pulse energy of (b) 2.4 nJ and (c) 3.2 nJ.

# 3.3 Stability of Mode-Locked Operation

The stability of our self-starting ML-TDFL is characterized by operating it in a laboratory environment and monitoring the output power and optical spectrum for 6 h. Fig. 10 shows good output power stability with a small fluctuation of  $\pm 1\%$ , primarily originated from variations in the pump source during the experiment. There was no active stabilization of temperature for the mode-locked cavity during the measurement, hence periodic temperature variations induced by the air conditioning system in the laboratory might also influence the temperature of the gain fiber and hence affect the laser output. The output spectrum acquired at a 1h intervals, exhibits good repeatability, as shown in Fig. 11.

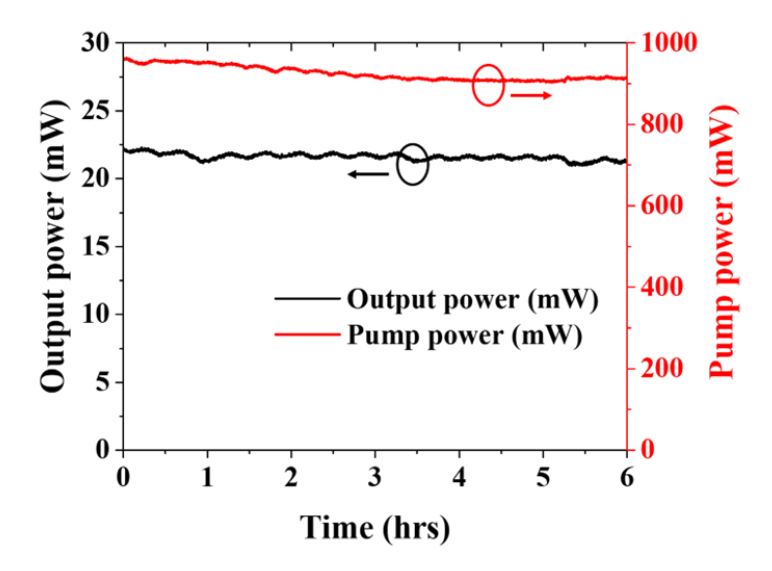


Fig. 10. Output power and pump power stability over 6h.

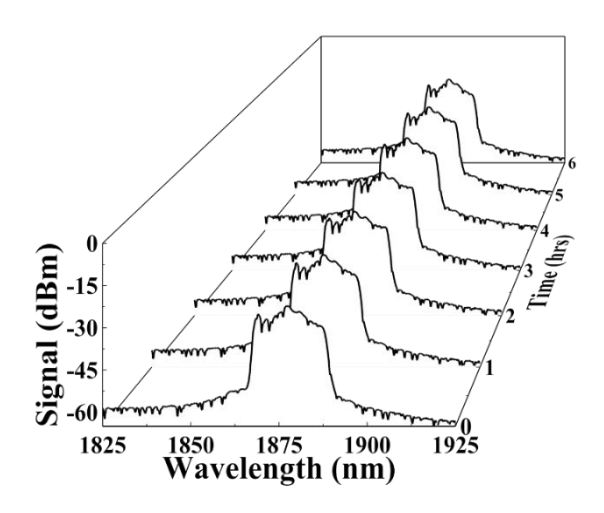


Fig. 11. Output spectrum for 6h measured at 1h time intervals.

#### 4. Conclusions

We reported a fully fiberized, environmentally stable, dissipative-soliton ML-TDFL operating at 1876 nm based on PM fibers. To the best of our knowledge, this is the first demonstration of a nJ-energy-level, all-PM dissipative-soliton ML-TDFL using commercially available fibers as DCF and a SWNT based SA. With a net-cavity dispersion of 0.01 ps², our ML-TDFL provides an output pulse energy of 1.1 nJ. The output pulses have a duration of 4.2 ps and can be compressed to 391 fs, under a Gaussian pulse-shape assumption, using a grating-based compressor. The net-cavity dispersion can be adjusted to achieve a higher pulse energy of 3.2 nJ, with a compressed pulse duration of 566 fs. Stable output pulse properties of the turn-key ML-TDFL was demonstrated. Due to its fully fiberized geometry and environmental insensitivity, our ML-TDFL could serve as a reliable source for multiphoton imaging in biomedical applications.

## 5. Funding

This work was supported by Engineering and Physical Sciences Research Council (EPSRC) grants EP/T020997/1,EP/V038036/1,EP/P030181/1, EP/K01711X/1,EP/K017144/1,EP/N010345/1, EP/L016087/1, EP/V000055/1, EP/X015742/1 and EU CHARM.

# 6. Data availability

Data are available at DOI: https://doi.org/10.5258/SOTON/D3443

#### 7. References

- [1] D. Grassani, E. Tagkoudi, H.R. Guo, C. Herkommer, F. Yang, T.J. Kippenberg, C.S. Bres, Mid infrared gas spectroscopy using efficient fiber laser driven photonic chip-based supercontinuum, Nat Commun 10 (2019).
- [2] B. Voisiat, D. Gaponov, P. Gečys, L. Lavoute, M. Silva, A. Hideur, N. Ducros, G. Račiukaitis, Material processing with ultra-short pulse lasers working in 2 µm wavelength range, Proc.SPIE, 2015, p. 935014.
- [3] C.W. Rudy, M.J.F. Digonnet, R.L. Byer, Advances in 2-µm Tm-doped mode-locked fiber lasers, Opt Fiber Technol 20(6) (2014) 642-649.
- [4] N.G. Horton, K. Wang, D. Kobat, C.G. Clark, F.W. Wise, C.B. Schaffer, C. Xu, In vivo three-photon microscopy of subcortical structures within an intact mouse brain, Nat Photonics 7(3) (2013).
- [5] S. Golovynskyi, I. Golovynska, L.I. Stepanova, O.I. Datsenko, L. Liu, J. Qu, T.Y. Ohulchanskyy, Optical windows for head tissues in near-infrared and short-wave infrared regions: Approaching transcranial light applications, J Biophotonics 11(12) (2018) e201800141.
- [6] D. Creeden, B.R. Johnson, G.A. Rines, S.D. Setzler, High power resonant pumping of Tm-doped fiber amplifiers in core- and cladding-pumped configurations, Opt Express 22(23) (2014) 29067-80.
- [7] J. Aubrecht, P. Peterka, P. Honzatko, O. Moravec, M. Kamradek, I. Kasik, Broadband thulium-doped fiber ASE source, Opt Lett 45(8) (2020) 2164-2167.
- [8] D.C. Kirsch, S. Chen, R. Sidharthan, Y. Chen, S. Yoo, M. Chernysheva, Short-wave IR ultrafast fiber laser systems: Current challenges and prospective applications, J Appl Phys 128(18) (2020).
- [9] Y. Nomura, H. Murakoshi, T. Fuji, Short-wavelength, ultrafast thulium-doped fiber laser system for three-photon microscopy, OSA Continuum 3(6) (2020) 1428-1435.

- [10] D. Xu, K.N. Bourdakos, A. Crisford, P. Johnson, I. Abughazaleh, P. Srisamran, R.O.C. Oreffo, S. Mahajan, D.J. Richardson, L. Xu, All-fiberized 1840-nm femtosecond thulium fiber laser for label-free nonlinear microscopy, Biomed Opt Express 14(9) (2023) 4520-4530.
- [11] S. Kobtsev, S. Smirnov, S. Kukarin, S. Turitsyn, Mode-locked fiber lasers with significant variability of generation regimes, Opt Fiber Technol 20(6) (2014) 615-620.
- [12] R.I. Woodward, Dispersion engineering of mode-locked fibre lasers, J Optics 20(3) (2018).
- [13] N. Kuse, J. Jiang, C.C. Lee, T.R. Schibli, M.E. Fermann, All polarization-maintaining Er fiber-based optical frequency combs with nonlinear amplifying loop mirror, Opt Express 24(3) (2016) 3095-102.
- [14] M.C. Li, L.H. Liu, T.P. Xiao, J.J. Xue, L.T. Liang, H.L. Wang, M. Xiong, Single-polarization polarization maintaining optical fiber with large stress birefringence and high homogeneity, Appl Phys Lett 89(10) (2006).
- [15] E. Baumann, F.R. Giorgetta, J.W. Nicholson, W.C. Swann, I. Coddington, N.R. Newbury, Highperformance, vibration-immune, fiber-laser frequency comb, Opt Lett 34(5) (2009) 638-640.
- [16] J. Noda, K. Okamoto, Y. Sasaki, Polarization-Maintaining Fibers and Their Applications, J Lightwave Technol 4(8) (1986) 1071-1089.
- [17] M. Michalska, Dispersion managed thulium-doped fiber laser mode-locked by the nonlinear loop mirror, Opt Laser Technol 138 (2021).
- [18] G. Sobon, J. Sotor, I. Pasternak, A. Krajewska, W. Strupinski, K.M. Abramski, All-polarization maintaining, graphene-based femtosecond Tm-doped all-fiber laser, Opt Express 23(7) (2015) 9339-46.
- [19] G. Sobon, A. Duzynska, M. Swiniarski, J. Judek, J. Sotor, M. Zdrojek, CNT-based saturable absorbers with scalable modulation depth for Thulium-doped fiber lasers operating at 1.9 µm, Sci Rep 7 (2017) 45491.
- [20] C. Cuadrado-Laborde, J.L. Cruz, A. Diez, M.V. Andres, Passively Modelocked All-PM Thulium-Doped Fiber Laser at 2.07 µm, IEEE Photonics J 14(4) (2022).
- [21] C. Huang, C. Wang, W. Shang, N. Yang, Y. Tang, J. Xu, Developing high energy dissipative soliton fiber lasers at 2 micron, Sci Rep 5 (2015) 13680.
- [22] J. Sotor, J. Bogusławski, T. Martynkien, P. Mergo, A. Krajewska, A. Przewłoka, W. StrupiŃski, G. SoboŃ, All-polarization-maintaining, stretched-pulse Tm-doped fiber laser, mode-locked by a graphene saturable absorber, Opt Lett 42(8) (2017) 1592-1595.
- [23] N. Zhang, W.Q. Jiang, Y.F. Meng, F.Q. Wang, All-polarization-maintaining mode-locked thulium-doped femtosecond laser at 1.7 µm, Opt Continuum 2(5) (2023) 1013-1019.
- [24] W.H. Renninger, A. Chong, F.W. Wise, Pulse Shaping and Evolution in Normal-Dispersion Mode-Locked Fiber Lasers, IEEE J Sel Top Quantum Electron 18(1) (2012) 389-398.
- [25] P. Grelu, N. Akhmediev, Dissipative solitons for mode-locked lasers, Nature Photonics 6(2) (2012) 84-92.
- [26] B. Gao, R.H. Zhang, J.Y. Huo, C.Y. Ma, Y. Han, Q.R. Hou, F. Deng, G. Wu, Y.Q. Ge, Generation and categories of solitons in various mode-locked fiber lasers, Optik 220 (2020).
- [27] C. Huang, Q. Wang, J. Geng, T. Luo, R. Liang, S. Jiang, All-PM Dissipative Soliton Fiber Laser at 2-Micron, Laser Congress 2017 (ASSL, LAC), Optica Publishing Group, Nagoya, Aichi, 2017, p. JTu2A.22.
- [28] B. Lyot, Optical apparatus with wide field using interference of polarized light, C. R. Acad. Sci. Paris 197 (1933) 1593.
- [29] Z.J. Yan, C.B. Mou, H.S. Wang, K.M. Zhou, Y.S. Wang, W. Zhao, L. Zhang, All-fiber polarization interference filters based on 45 degrees-tilted fiber gratings, Opt Lett 37(3) (2012) 353-355.
- [30] J. Ye, J.M. Xu, J.X. Song, H.Y. Xu, H.S. Wu, H.W. Zhang, J.Y. Leng, P. Zhou, Power scalability of linearly polarized random fiber laser through polarization-rotation-based Raman gain manipulation, Opt. Express 26(18) (2018) 22894-22903.
- [31] K. Ozgoren, F.O. Ilday, All-fiber all-normal dispersion laser with a fiber-based Lyot filter, Opt Lett 35(8) (2010) 1296-1298.
- [32] Y. Zhu, Z. Cui, X. Sun, T. Shirahata, L. Jin, S. Yamashita, S.Y. Set, Fiber-based dynamically tunable Lyot filter for dual-wavelength and tunable single-wavelength mode-locking of fiber lasers, Opt Express 28(19) (2020) 27250-27257.
- [33] I. Armas-Rivera, L.A. Rodríguez-Morales, S. Cortés-López, M. Durán-Sánchez, M.V. Andrés, B. Ibarra-Escamilla, All-fiber fully controlled Lyot filter based on bend-induced linear birefringence with tension, Opt Laser Technol 175 (2024).
- [34] M.L. Dai, B.W. Liu, T. Shirahata, X.N. Sun, S.Y. Set, S. Yamashita, All-polarization-maintaining, efficiently wavelength-tunable, Er-doped mode-locked fiber laser with a compact reflective Lyot filter, Opt. Express 31(17) (2023) 27810-27820.
- [35] T. Hasan, Z.P. Sun, F.Q. Wang, F. Bonaccorso, P.H. Tan, A.G. Rozhin, A.C. Ferrari, Nanotube-Polymer Composites for Ultrafast Photonics, Adv Mater 21(38-39) (2009) 3874-3899.
- [36] P. Ciacka, A. Rampur, A. Heidt, T. Feurer, M. Klimczak, Dispersion measurement of ultra-high numerical aperture fibers covering thulium, holmium, and erbium emission wavelengths, J Opt Soc Am B 35(6) (2018) 1301-1307.

- [37] K. Watanabe, Y. Zhou, Y. Sakakibara, T. Saito, N. Nishizawa, Dispersion-managed, high-power, Tm-doped ultrashort pulse fiber laser using single-wall-carbon-nanotube polyimide film, OSA Continuum 4(1) (2021) 137-148
- [38] H. Telg, J. Maultzsch, S. Reich, F. Hennrich, C. Thomsen, Chirality distribution and transition energies of carbon nanotubes, Phys Rev Lett 93(17) (2004) 177401.
- [39] A.C. Ferrari, J. Robertson, Interpretation of Raman spectra of disordered and amorphous carbon, Phys Rev B 61(20) (2000) 14095-14107.
- [40] R.B. Weisman, S.M. Bachilo, Dependence of optical transition energies on structure for single-walled carbon nanotubes in aqueous suspension: An empirical Kataura plot, Nano Lett 3(9) (2003) 1235-1238.
- [41] T.R. Schibli, E.R. Thoen, F.X. Kärtner, E.P. Ippen, Suppression of Q-switched mode Locking and break-up into multiple pulses by inverse saturable absorption, Appl Phys B 70 (2000) S41-S49.
- [42] A. Chong, W.H. Renninger, F.W. Wise, Properties of normal-dispersion femtosecond fiber lasers, J Opt Soc Am B 25(2) (2008) 140-148.
- [43] Q. Lin, I. Sorokina, High-order dispersion effects in solitary mode-locked lasers: side-band generation, Opt Commun 153(4-6) (1998) 285-288.
- [44] Y. Li, L. Wang, Y. Kang, X. Guo, L. Tong, Microfiber-enabled dissipative soliton fiber laser at 2  $\mu$ m, Opt Lett 43(24) (2018) 6105-6108.